Limnol. Oceanogr., 44(1), 1999, 166–177

Physical constraints of chemoreception in foraging copepods

Paul A. Moore
Laboratory for Sensory Ecology, Department of Biological Sciences, Bowling Green State University, Bowling Green, Ohio 43403

David M. Fields
Georgia Institute of Technology, School of Biology, Atlanta, Georgia 30332

Jeannette Yen
Marine Sciences Research Center, State University of New York, Stony Brook, New York 11794-5000

Abstract

The small-scale spatial and temporal dynamics of phycosphere-sized chemical signals entrained within the feeding current of copepods is quantified here by combining flow visualization techniques with electrochemical technology (IVEC-10). Using the 30-μm electrochemical probe sampling at 50 Hz and the velocity gradients created by two marine copepods, we evaluated how odor deformation improves the potential for remote chemoreception. Our data show that when shear is strong, as found in the feeding current of an omnivore, *Pleuromamma xiphias,* elongation of the chemical signal is greater than that found for an odor signal entrained in the low-shear feeding current of a carnivore, *Euchaeta rimana.* Furthermore, within the feeding current of a single species, *E. rimana,* certain areas provided greater potential for remote chemoreception. These results support the hypotheses that chemical signals are deformed by the feeding current and that the feeding current structure enhances signal detection. The deformation of the odor field within the laminar feeding current provides a leading edge that gives a chemosensitive copepod early warning of an approaching odor source. By sensing the leading edge, a copepod could have a few hundred milliseconds to reorient itself with respect to the odor source. Advance warning improves the probability of successful behavior in response to signal sources such as prey, predators, and mates.

Copepods live in a nutritionally dilute aquatic environment. Their foods, algae and microzooplankton (2–100 μm), are typically dispersed at concentrations of 10^3 ind ml^{-1}, and they themselves occur at densities of <1 ind ml^{-1}. If a copepod is considered a passive feeder, it would need to process large quantities of water to obtain the ''little part of value'': the food (Strickler 1985). Instead, morphological, physiological, and behavioral observations support the use of sensory reception in the location and identification of items of interest. Copepods have both mechano- and chemoreceptors on their first antennules, other cephalic appendages, and mouthparts (Strickler and Bal 1973; Friedman 1980; Dourdeville 1981; Weatherby et al. 1994). When feeding, copepods create an organized flow field that passes across their sensors, allowing copepods to scan up to several hundred milliliters of water a day (Cannon 1928; Koehl and Strickler 1981; Strickler 1985; Yen et al. 1991; Fields and Yen 1993). The use of mechanoreception in predator–prey interactions has been documented (Strickler and Bal 1973; Zaret 1980; Gill and Poulet 1986; Yen and Nicoll 1990; Yen and Fields 1992; Fields 1996; Wong 1996). The stimulus threshold for the depolarization of mechanoreceptors of the first antennules (Yen et al. 1992) as well as for the initiation of behavior (Yen and Fields 1992; Fields and Yen 1997) has been measured for several species. Similarly, studies on the chemoreceptive abilities of copepods have shown that they detect the odor of food patches (Poulet and Marsot 1978) and follow chemical trails of mates (Yen et al. 1998). Other behavioral studies have found that copepods increase the speed of their feeding appendages in response to amino acids (Gill and Poulet 1988). In these cases, encounter rate with the item of interest, food or mate, is improved by chemoreceptive ability. However, the mechanism underlying their ability to detect and respond to chemical signals in their environment is relatively unexplored. In this study, we present a novel approach to understanding the relationship between the feeding current structure of copepods and their ability to detect and orient to chemical signals in their environment.

The role of the flow field in chemoreception—The encounter rate with food particles is, in part, determined by the magnitude of the relative motion between the copepod's body and the surrounding fluid (Rothschild and Osborn 1988). Moving through the water, as opposed to moving water over the sensors, has the same effect on the encounter rate. However, these contrasting situations can have very different implications on the types of signals perceived by the copepod (Fields 1996; Yen and Strickler 1996). One type of signal is the chemical gradient created and maintained by Fickian diffusion that surrounds organic objects (Lazier and

Acknowledgments

The authors would like to thank Akira Okubo and J. Rudi Strickler for initiating this collaboration and providing assistance and ideas. Troy Keller and George Bullerjahn and two anonymous reviewers have provided numerous insightful comments on the structure and style of the manuscript. We would also like to thank Jerry Liu and Michael Doall for assistance during experiments. This work is funded by NSF grants OCE-9314474 and IBN-9514492 to P.A.M. and ONR contract N-0001492J1690 to J.Y.

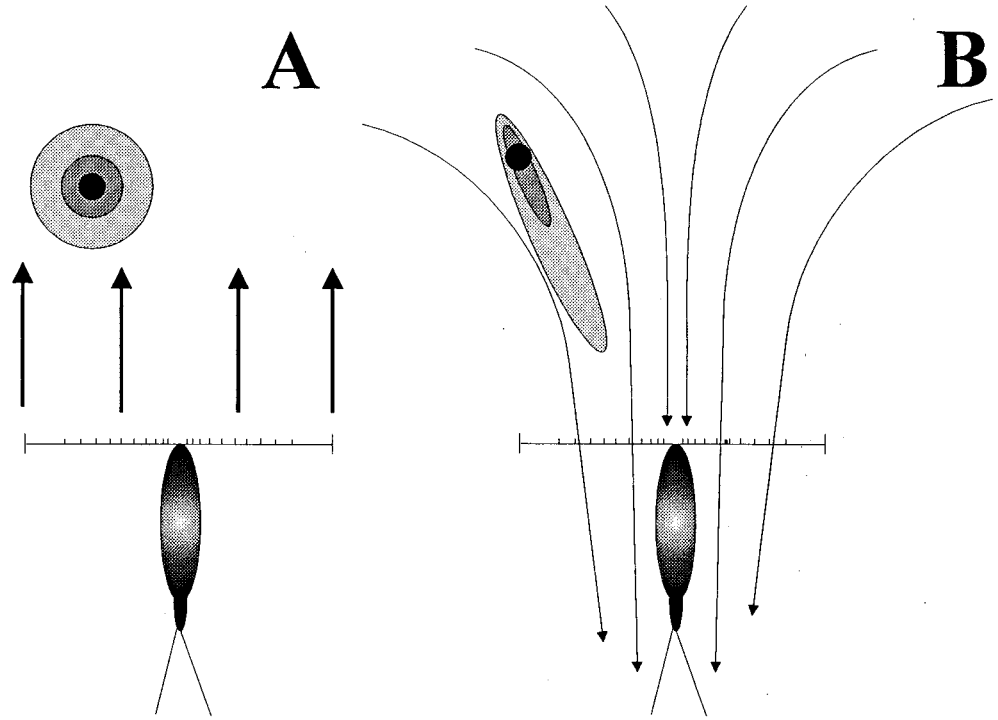

Fig. 1. Schematic diagrams of the hypothetical changes in odor structure surrounding an algal cell (shaded circles) under (A) no shear, and (B) sheared flow conditions. Arrows indicate motion of the copepod (thick arrows) and water (thin arrows).

Mann 1989). When undisturbed by advective forces, the shape of the chemical gradient, or phycosphere, remains a series of concentric spheres defined by the concentration gradient. When a copepod moving at the speed of the feeding current approaches such an object, the phycosphere surrounding the object is minimally disturbed. In this scenario, the reactive distance is limited by the processes involved in molecular diffusion and the rate of chemical exudation (Fig. 1A). However, if the copepod remains stationary in the water column, by balancing the force of the feeding current with the forces due to gravity and drag (Strickler 1982), the created sheared feeding current causes relative motion between the object and its surrounding chemical gradients (Fig. 1B). This shearing will increase the distance between the leading edge of the chemical gradient and the object, allowing more time for the animal to respond (Csanady 1980; Okubo 1980; Andrews 1983). Since the feeding currents are generated at low Reynolds numbers, flow is laminar and chemical dispersion is due to both molecular diffusion and advection. Flow streamlines intersect the specific sensors from a discrete origin in space, making a predictable, organized sensory environment (Strickler 1985; Fields and Yen 1993; Yen and Strickler 1996). Therefore, the potential for remote chemoreception is maximized when chemical sources are entrained in a flow field rather than approached by a moving copepod.

Andrews (1983) modeled the deformation of chemical signals within feeding currents. He defined the ''active space'' as the chemical field around an alga where exudate concentrations are sufficiently high to elicit a behavioral response. Two types of shear are found within a flow field (*see Table 1*). His model shows that both types of shear increase the separation between the leading edge of the chemical signal and the particle. However, while longitudinal shear increases the separation distance, it does not increase the amount of time the animal has to respond to a particle because of equal acceleration along adjacent streamlines. In contrast, transverse shear changes the relative motion of the source of the chemical signal (the alga in this case) and a given concentration isoline, thus increasing the physical and the temporal separation between the leading edge of odor and alga. (For further details, *see* fig. 5.11 in Csanady 1980 and fig. 2.11 in Okubo 1980.) Therefore, Andrews (1983) suggests, animals that generate feeding currents with high transverse shear create an elongated active space; this active space triggers chemoreceptors, leading to a behavioral response in advance of an approaching alga. The structure of the active space can vary between copepods since species differ in swimming orientation, appendage morphology, and specific gravity (Tiselius and Jonsson 1990; Bundy and Paffenhofer 1996; Fields 1996). By using two copepod species (*P. xiphias* and *E. rimana*) as tools to examine the effect of different feeding current geometry on the deformation of entrained chemical signal, we examine the implications of Andrews' findings (1983).

Methods

Zooplankton collection—The dynamics of chemical signals entrained within copepod feeding currents were exam-

Table 1. Equations used to define temporal and spatial relationships within the velocity gradient of copepod feeding currents. Longitudinal shear (S_l) describes relative motion of the fluid along a streamline (associated with the fluid acceleration), while transverse shear (S_t) describes the relative motion of the fluid along adjacent streamlines. The velocity in the horizontal direction (x) is U, and the velocity in the vertical direction (y) is V. The velocity of the water along a streamline is V_s, where s is the distance from the copepod's antennules along the streamline to the center of the chemical bolus and a and b are constants determined by numerical iteration. The Peclet number (Pe) is the ratio of advective to diffusive forces, determined from the distance between the source and receiver (L) and the diffusion coefficient (D_m). The characteristic diffusion length (r) computes the distance traveled by a diffusing chemical over time (t).

Equations	
$S_l = \frac{\delta U}{\delta x} + \frac{\delta V}{\delta y}$	Eq. 1
$S_t = \frac{\delta V}{\delta x} + \frac{\delta U}{\delta y}$	Eq. 2
$V = a(s + 1)^b$	Eq. 3
$\mathrm{Pe} = V_s L / D_m$	Eq. 4
$r = \sqrt{4 D_m t}$	Eq. 5

ined for two oceanic species. *E. rimana* (length 2.5 mm), a surface-dwelling carnivorous copepod, and *P. xiphias* (length 5.5 mm), a strong vertical-migrating omnivore, were collected at the Natural Energy Laboratory of Hawaii Authority (NELHA) located in Kailua-Kona, Hawaii, from 10 December to 3 January 1994. The copepods were transported to Stony Brook, New York, for experiments. Animals were maintained in laboratory incubators at 20°C. Prior to filming, animals were tethered to a tin-coated wire (0.15 mm in diameter), suspending them in view of two video cameras.

Video imaging—Filming was done using a Schlieren optical pathway (Strickler 1985; Strickler and Hwang 1997) in a fixed frame with a single HeNe (632 nm) laser as a light source (Yen and Fields 1992). The tethered copepod was positioned within the center of a cubic 300-ml vessel and filmed from perpendicular angles to simultaneously record the three-dimensional coordinates of the copepods' antennules, particle trajectories, stimulus pipette, and electrode. Images were captured by two synchronized Pulnix video cameras (TM-745) and stored using two Panasonic AG-1960 S-VHS recorders. Video recordings were done at 60 Hz and analyzed field by field using image analysis software (Optimus, Bioscan). During these sequences when the copepod created its flow field, the tether did not move. Video sequences where the tether moved as a result of the copepod flicking the antennules, performing escapes, or other nonfeeding current behavior were excluded from further analysis.

Flow field analysis—The trajectories of small (21 μm), inert, neutrally buoyant polystyrene spheres (PolyScience) were used as markers for fluid motion in the copepods' feeding currents. The animals were positioned such that the dorsal view was filmed by one camera and the lateral view filmed by the other. The dorsal view was used to determine particle position in the one of the horizontal directions (x) and in the vertical direction (z). The lateral view was used to track particle position in the other horizontal direction (y) and in the vertical direction (z). Particle matching was accomplished by comparing the vertical location of each particle trajectory in the two perpendicular views. To create relatively planer views of the fluid velocity and shear, a corridor 1 mm wide for *P. xiphias* and 250 μm wide for *E. rimana* was defined in the lateral view along the sagittal plane (Fig. 2). The corridor was centered over the body such that half was ventral and the other half dorsal to the body, extending at least one body length anterior. Particles that maintained their trajectories within this corridor then were tracked in the dorsal view to determine their change in space over time. It is important to note that by using the corridor, we tracked particles that traveled along the plane in the two-dimensional manner, not particles that passed through the plane. There were no particles entering the corridor within one body length distance that did not remain in the corridor. Nor were there particles entering the corridor at a distance of less than one body length. For the animals used in this study, flows entrained above the antennules passed over the antennules.

By using the corridor method to calculate velocity (as described by Fields and Yen [1993]), the maximum error associated with compressing a three-dimensional volume onto a two-dimensional plane was a 4% underestimation of the actual three-dimensional velocity.

The velocity was calculated as the distance traveled over a measured time interval, and a two-dimensional Cartesian coordinate was assigned to the midpoint of the velocity vector. To diminish the error associated with assigning the magnitude of the velocity to the midpoint of large velocity vectors, different time scales were used depending on the distance traveled. For those water velocities slower than 1.00 mm s^{-1}, one-third of a second was used, from 1.00 mm s^{-1} to 3.50 mm s^{-1}, and over 3.50 mm s^{-1}, the distance traveled over one-sixth and one-thirtieth of a second, respectively, were used. The fluid velocity was analyzed using the contouring software package SURFER. Profiles of flow velocity along the antennules were taken from contoured data and calculated as averages between the left and right antennules. To calculate fluid shear (Eq. 1), velocity data were extracted from contoured data at 20-μm intervals. Calculated shear values were contoured and the profiles extracted from contoured data.

Electrochemical electrodes and recording procedures—Single carbon fiber electrodes were used for all recordings and selected based on a linear calibration curve for the tracer chemical (dopamine). The sampling area of the electrode is determined by the exposed carbon epoxy surface area (Adams 1969; Gerhardt et al. 1987). All carbon fiber electrodes were 30 μm in diameter and 50–75 μm long. Electrochemical recordings were made at 50 Hz using standard principles with the IVEC-10 (In Vivo Electrochemistry Computer Sys-

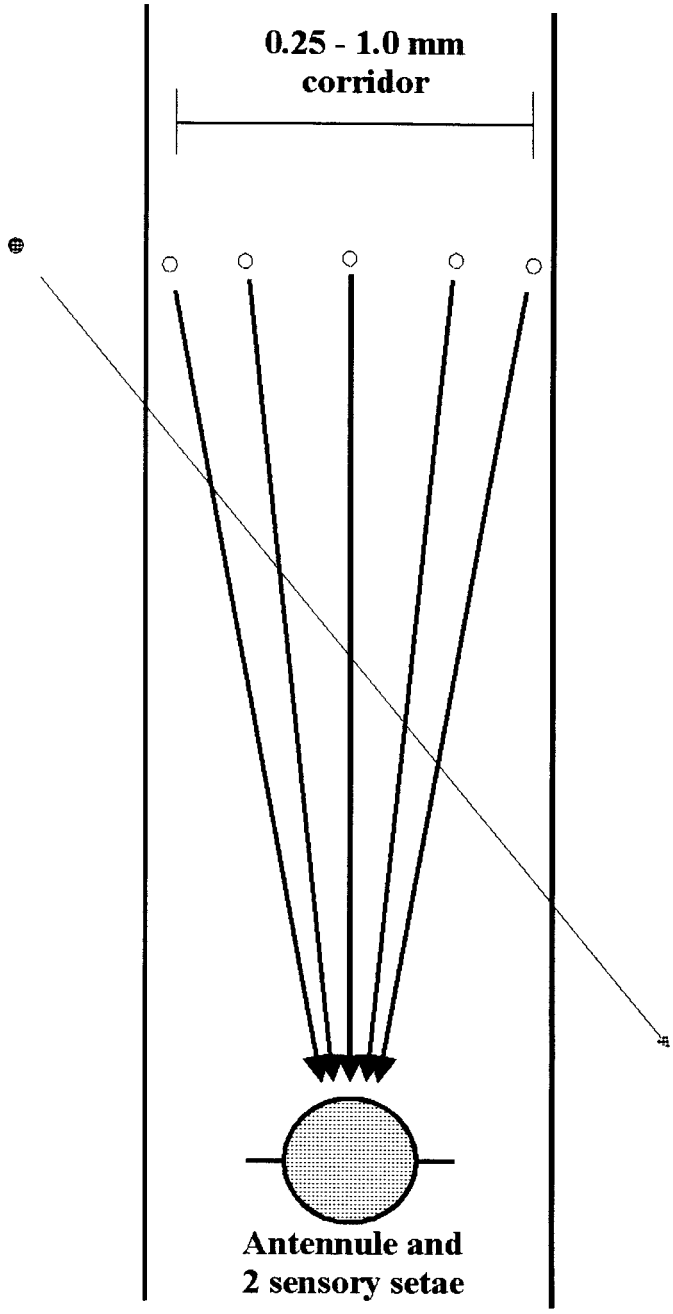

Fig. 2. View of the flow corridor (0.25–1.0 mm) within the sagittal plane anterior to the tethered copepod. Only trajectories (solid lines) of those particles (small open circles) remaining within the corridor for at least one body length (2.5–5 mm) anterior to and intersecting the antennules (100–300 μm; shaded circle) and sensory setae (10–100 μm; horizontal lines) were used in flow velocity measurements. Particles that passed through the corridor (solid gray lines) were not observed for the copepods studied.

tem, Medical Systems). A constant voltage of +0.55 V was applied to the electrode, and analog-to-digital conversions of the samples occurred at 4 kHz. Further details of recording and digitizing are explained elsewhere (Moore et al. 1989). Electrodes, calibrated in solutions of dopamine in filtered

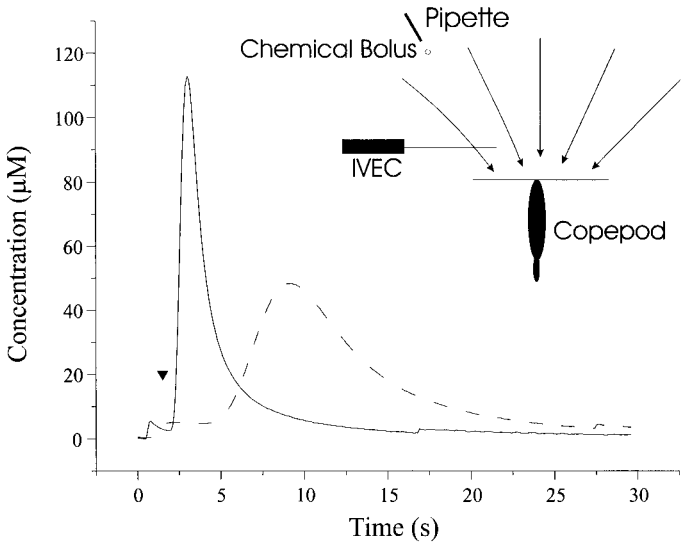

Fig. 3. Typical trace of chemical concentration as it passes the IVEC chemical sensor with the copepod present (solid line) and absent (dotted line). Triangle marks the time that the chemical bolus was released. Inset shows the spatial arrangement of the IVEC sensor, stimulus pipette, and copepod. The sensor was positioned along the streamlines connecting the introduced bolus to the copepod antennule.

seawater, exhibited excellent linearity over a concentration range of 10–2,000 micromolar (correlation coefficient; $r^2 > 0.97$). Tracer chemical (50 mM dopamine) was released from a 10-μm-diameter glass pipette using pressure ejection (Picosprizter, General Valve). Time-pressure parameters were kept constant throughout all trials at 4 ms at 5 psi. The release parameters minimized the amount of chemical transport due to the pressure ejection itself. They were also chosen so that the chemical bolus produced approximated the spatial dimension of potential copepod prey (e.g., an algal cell). Control studies were performed under identical conditions without the presence of a copepod. Absolute time between the pressure ejection, chemical detection, and the videotape was synchronized (within 20 ms) using a transistor-transistor logic (TTL) pulse and light-emitting diode light.

Electrode and odor source pipette positions (relative to the rostrum of the copepod) were obtained from the video using the method outlined above. The pipette was positioned at different locations from the copepod, designated as (x, z) where x denotes distance to the left of the copepod's rostrum and z the distance above the rostrum ($\pm$0.01 mm). For *P. xiphias*, the pipette was placed at 2.86 mm, 2.48 mm, while for *E. rimana*, odor was introduced from two locations: 0.88 mm, 1.17 mm and 1.76 mm, 0.86 mm. Twenty-five to 30 positions were sampled four times (replicates) in a two-dimensional array (x, z) distal to the antennules of the copepods. These measurements resulted in an odor profile (concentration vs. time plot; Fig. 3) for each spatial position and replication. Replications for each spatial site were synchronized using the TTL mark and averaged. Two-dimensional (x, z) odor contours were constructed using the mean concentration at three time points (0.5, 1, and 2 s after ejection).

Contours were constructed from 25–30 spatial samples and were fitted using an exponential decay function. For display purposes, concentration levels were contoured relative to the maximum concentration within each plot. This normalization of concentration levels was done to simulate a constantly leaking or emitting odor source. Absolute concentration levels decayed with distance from the pipette due to diffusion and advection. Since algal cells will act like a constant odor source by leaking or emitting chemicals (Carr 1988), contouring concentration levels relative to the maximum concentration (always located at the center of the chemical bolus) will mimic more closely those contours from a real environmental source. Jackson (1989) has used these assumptions of a constant concentration over time to model concentration of metabolites in falling algae. The contours generated using our empirical data (Figs. 6, 7) correspond to those modeled by Jackson (1989: *see fig. 1*).

Forewarning times and detection distances—Algal cells are entrained within the feeding currents of copepods. As the distance between the algal cell and the copepod decreases, the animal is exposed to a greater chemical concentration of algal exudates. When the exudate surrounding the alga reaches the behavioral threshold of the animal, it signals the copepod of the cell's proximity. This threshold concentration surrounding the alga forms the leading edge of the algal cell exudate. Thus, remote detection of the leading edge of the chemical gradient provides a forewarning for the copepod as to the arrival of the alga cell. The amount of forewarning is calculated as the difference between the time of arrival of a leading edge of the chemical gradient and the actual arrival of the model alga cell (center of the chemical bolus). To calculate the advance warning time available to the copepod, the velocity profile along the chemical streamline is fit to the power function (*see Table 1, Eq. 3*). The average speed of the chemical bolus is determined by integrating the velocity-distance curve for the values between each concentration isoline and the antennules of the copepod and dividing that value by the total distance traveled. The distance traveled divided by the average speed provides the travel time.

Results

Flow fields of tethered copepods—We recognize that tethering can distort the flow field, creating higher flow velocities with greater shear than that found in the feeding current of a freely swimming plankter (Emlet 1990). It is difficult to discern whether a tethered copepod is swimming against the tether, ''hovering,'' or attempting to sink, and we acknowledge that the flow magnitude and specific shape may vary depending on the behavior pattern exhibited by the copepods and the body orientation. Despite these effects, marked differences in the general patterns can be used to characterize species-specific distinctions. The ''value'' of using feeding current data from tethered animals has been the source of considerable debate (Gallager 1993; Bundy and Paffenhofer 1996). Yet the collection of the type of data in this paper is presently not possible without restraining the animals. Therefore, although there are inherent problems with tethering copepods, we suggest that the present data—comparing species that produce different tethered feeding currents—be used as a tool to provide insight into the physical constraints required for effective chemoreception and the physiological properties of copepod chemoreceptors. Tethering allowed the copepod feeding current to be used as a source for biologically relevant flow. The tethered copepod generated a flow field that changed little over time yet displayed spatial variation across the field. From these temporally stable yet spatially variable feeding currents, we can surmise how differences in shear, occurring at appropriate temporal and spatial scales of copepods, cause variations in odor deformation.

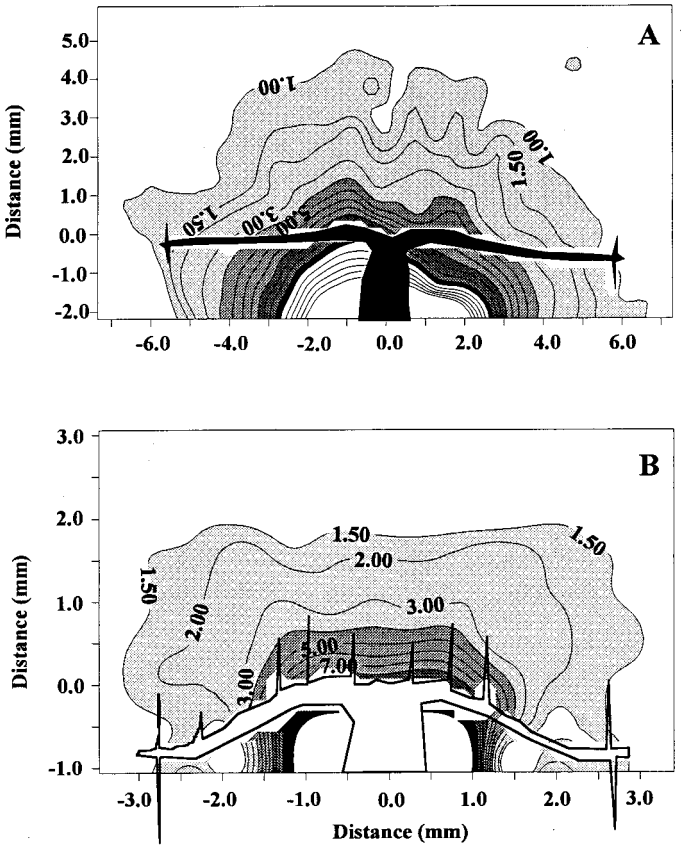

Fig. 4. Flow contours of the feeding current of (A) *P. xiphias*, and (B) *E. rimana.* Contour intervals are 1 mm s^{-1} (0.5 mm s^{-1} for flow rates between 1 and 2 mm s^{-1}). Note change in scale of both axes.

The flow velocity contours for tethered *P. xiphias* and *E. rimana* are shown in Fig. 4. Within the plane bisecting the copepod dorsal ventrally and extending anteriorly from the rostrum and laterally to the distal tips of the antennules, we found the size and shape of the feeding current differed significantly between the two species. The maximum speed along the antennules of *P. xiphias* was near the rostrum, with a rapid decrease in speed more laterally. The decrease in flow speed was greatest (30%) 0.25–0.75 mm along the antennules. Over the subsequent 5 mm, flow speed decreased 60%, so that flow at the distal tips was 0.7 mm s^{-1}. The profile of flow speed 1 mm anterior to the antennules was similar to that along the antennules. The rate of decrease in

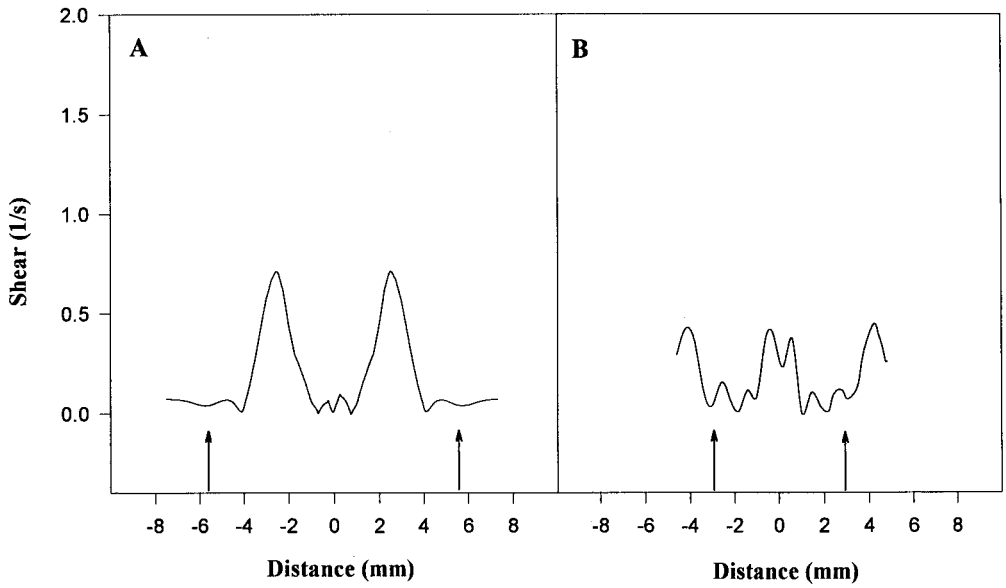

Fig. 5. Profile of flow shear along the antennules for (A) *P. xiphias*, and (B) *E. rimana*. Distances are measured from the rostrum. Vertical arrows represent the distal tips of the first antennules.

fluid speed along the antennules is a measure of the two-dimensional transverse shear rates in the fluid (Eq. 1). The maximum shear rates along the antennules were found 0.25–0.75 mm from the rostrum (Fig. 5A). At 1 mm above the antennules, maximum shear rates were located 1.5–2.5 mm from the rostrum. It is in these regions of maximum shear that we would expect the greatest degree of stretching of a chemical bolus entrained in the feeding current.

The water speed profiles of *E. rimana* contrasted sharply with those of *P. xiphias*. Maximum flow speed for *E. rimana* occurred between 0.5 mm and 1.0 mm laterally to the rostrum, creating a slight bimodal distribution of velocity along the antennules. At distances along the antennules >1.0 mm from the rostrum, water speed decreased rapidly with increased distance. Highest transverse shear was between 1.0 and 2.0 mm along the antennules. One millimeter above the antennules, however, the profile of flow speed was nearly monotonic at ca. 2.5 mm s^{-1} and showed little or no transverse shear (Fig. 5B). Because of the lack of shear, relatively little distortion of incoming chemical signals 1 mm above the antennules would be expected for *E. rimana*.

In addition to the higher shear rates, the sphere of influence of the feeding current of *P. xiphias* was considerably different from that of *E. rimana*. Although both animals showed similar maximum speeds of $\sim$10 mm s^{-1} within the region of the feeding currents above the antennules, the effects of the generated flow field were detected much further for *P. xiphias*. For example, flow speeds for *P. xiphias* were found to exceed 5 mm s^{-1} at a distance of 3 mm from the rostrum, while for *E. rimana*, flow speeds had decreased to <1.5 mm s^{-1} at the same distance. *P. xiphias* has a larger sphere of influence because the volume transported is proportional to the product of the surface area and flow speed, and it also has a much larger surface area on its locomotory appendage than *E. rimana*. These maximum flow field velocities were those observed within the examined corridor; however, high-velocity streamlines are also known to cross receptors on the mouthparts. The tethered *P. xiphias* has a feeding current that is comprised of high-speed flow-entraining water from a large volume into a highly sheared flow field. This is in sharp contrast to the feeding current of the tethered *E. rimana*, which is comprised of low-speed flow-entraining water from a small volume into a minimally sheared flow field. The combined effects of these distinctions in flow speed and shear were examined for their influence on odor patch distortions and forewarning time.

Odor fields—Our study used a bolus (although a ring vortex may be a more accurate description) of dopamine to mimic an odor patch similar in dimensions to that of a phycosphere. A bolus, as created here, also could mimic an odor patch excreted by a zooplankter. The odor contours for the controls showed a uniform slow lateral and slightly elongated vertical distortion (Fig. 6). The center of maximum concentration remained around the pipette until the odor was evenly dispersed at >60 s. The difference in shape between true molecular diffusion (spherical) and that which was measured was due to the pressure ejection causing a deformation of the odor bolus and background convective fluid motion.

The odor field for *P. xiphias* showed a considerable difference over the control situation (Fig. 7, upper). In <2 s, the center of the odor field moved rapidly past the antennules of the copepod. The initial bolus was roughly spherical (Fig. 7; 0.5 s) but was quickly stretched along the x-, z-axes due to different flow velocities and different shear forces. After 1 s, the odor field has been stretched and pulled toward the rostrum of the copepod (Fig. 7; 1 s). The contour became almost oval in shape due to increased flow velocities toward the rostrum of the animal. By 2 s, the odor bolus had moved past the antennules into the area of highest shear, where it increased in width from 1.5 mm (at 1 s) to 2.4 mm.

The lower feeding current flow velocities of *E. rimana*

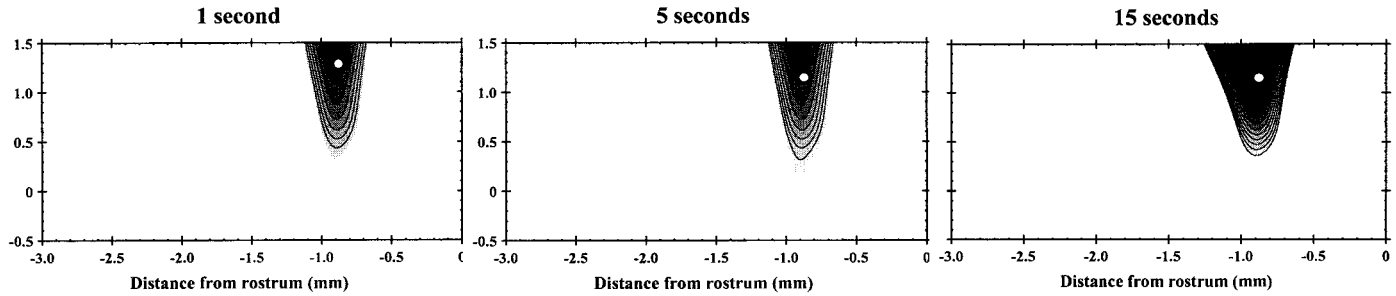

Fig. 6. Odor contours for the control situation (copepod absent with molecular diffusion, background convection, and pressure ejection acting) at 1, 5, and 15 s after ejection of odor bolus. Distances are shown as millimeters from the origin. Contour colors are spaced at 10% intervals relative to the maximum concentration within each plot (the center). Open circle is the location of the stimulus pipette. In other contour plots (Fig. 7), the rostrum of the copepod is located at the origin.

resulted in less lateral dispersion in distribution of odors than observed for *P. xiphias* (Fig. 7, middle). The contours were more spherical, and those closest to the center were deformed only after 2 s. At this point, the more oval fields had greater concentration gradients more medial to the animal's rostrum.

Different regions of *E. rimana*'s feeding current have different fluid structure. As a result, area-specific differences in the odor field deformation occurred when the chemical signals were injected into different parts of the *E. rimana* feeding current. In the slower region of the feeding current, the signal traveled much slower (Fig. 7, lower). After 2 s, the center of the chemical distribution had not yet reached the antennules, and the entire field was more spherical. Concentration contours were more evenly spaced, with little lateral deformation.

Remote detection—Advanced warning varies as a function of both fluid velocity and detection distance. Maximum fluid velocity along the plume path was comparable for both *P. xiphias* (Fig. 8A) and the more lateral path of *E. rimana* (Fig. 8B). Maximum velocity for both animals was about 10 mm s^{-1}, with speed decreasing as a function of distance. However, a comparison of fluid velocity for different regions of the flow field of *E. rimana* showed the water velocity within a plume path can be quite different, depending on location (compare Fig. 8B,C). For particles that approach from the proximal pipette location, fluid velocities ranged from 5 mm s^{-1} at 0.5-mm distance to a maximum of 10 mm s^{-1} when intersecting the antennules of the animal (Fig. 8C). In contrast, for particles that approach from the distal pipette location at similar distance from the animal's antennules, maximum fluid velocities were often $<$50% of those from the proximal pipette location.

The rate of increase in fluid speed along the plume path (longitudinal shear) was also greater for *P. xiphias* than for *E. rimana* (Table 2). Higher shear rates caused greater elongation of the plume as it approached the animal's sensors. Detection distance calculations (Eq. 3) suggested that *P. xiphias* could detect an approaching chemical bolus at a distance of 750 μm (Fig. 9A) with a detection threshold of 20% of the maximum concentration. The detection distance decreased with an increasing threshold concentration. In contrast, the feeding current of *E. rimana* gave a maximum detection distance of 400 μm for proximal particles (Fig. 9C) and only 250 μm for particles approaching from a more distal region (Fig. 9B).

Detection distance is only one facet of advanced warning information from chemical signals. The animal must have sufficient time to respond to the incoming alga. The actual time that the animal has to react to the particle is the interval from the moment of detection until the particle passes the capture area of the animal. Thus, the speed of the flow and sensitivity of the chemoreceptors set the amount of time the animal has to react. We calculated detection time from detection distance using the velocity profiles. These calculations showed that the particle path for *P. xiphias* provided the animal with up to 274 ms warning with an assumed detection threshold of 20% of maximum concentration (Fig. 10A). The warning time was 500% greater for *P. xiphias* than either path examined for *E. rimana* (Fig. 10B,C). There was little difference in warning time between the two path locations examined for *E. rimana.* Assuming a detection threshold of 20% of the maximum algal exudate concentration, the distance from the animal at which the particle could be detected was 100% greater (0.4 vs. 0.2 mm) if the chemical bolus approached from the proximal pipette position. This larger warning distance, however, was not manifested as an increase in the warning time since the odor traveled across this distance at a greater speed (compare Fig. 10B,C).

The degree of forewarning depends on the separation between the leading edge of the chemical signal and the alga. This warning distance is due to the combined effect of animal advection, background convection, and residual momentum from the pressure ejection of the odor bolus plus molecular diffusive forces. To assess the relative importance of advection vs. molecular diffusion, we examine the Peclet number (Table 1, Eq. 4). If this number is $>$1, then flow is more important than molecular diffusion in the movement of chemicals. In our controls with no animal-driven flow, the solute ''diffused'' 500 μm within 1 s (Fig. 6). Using the equation for the characteristic diffusion length (Table 1, Eq. 5), an apparent diffusion coefficient of 6×10^{-4} cm^2 s^{-1} was calculated. This coefficient represents solute transport in our controls due to molecular diffusion, background eddy diffusion, and pressure ejection. The Peclet number is 13–25, using the empirically determined value of D_m, an average flow velocity (V_s) of 2 mm s^{-1}, and a length of separation

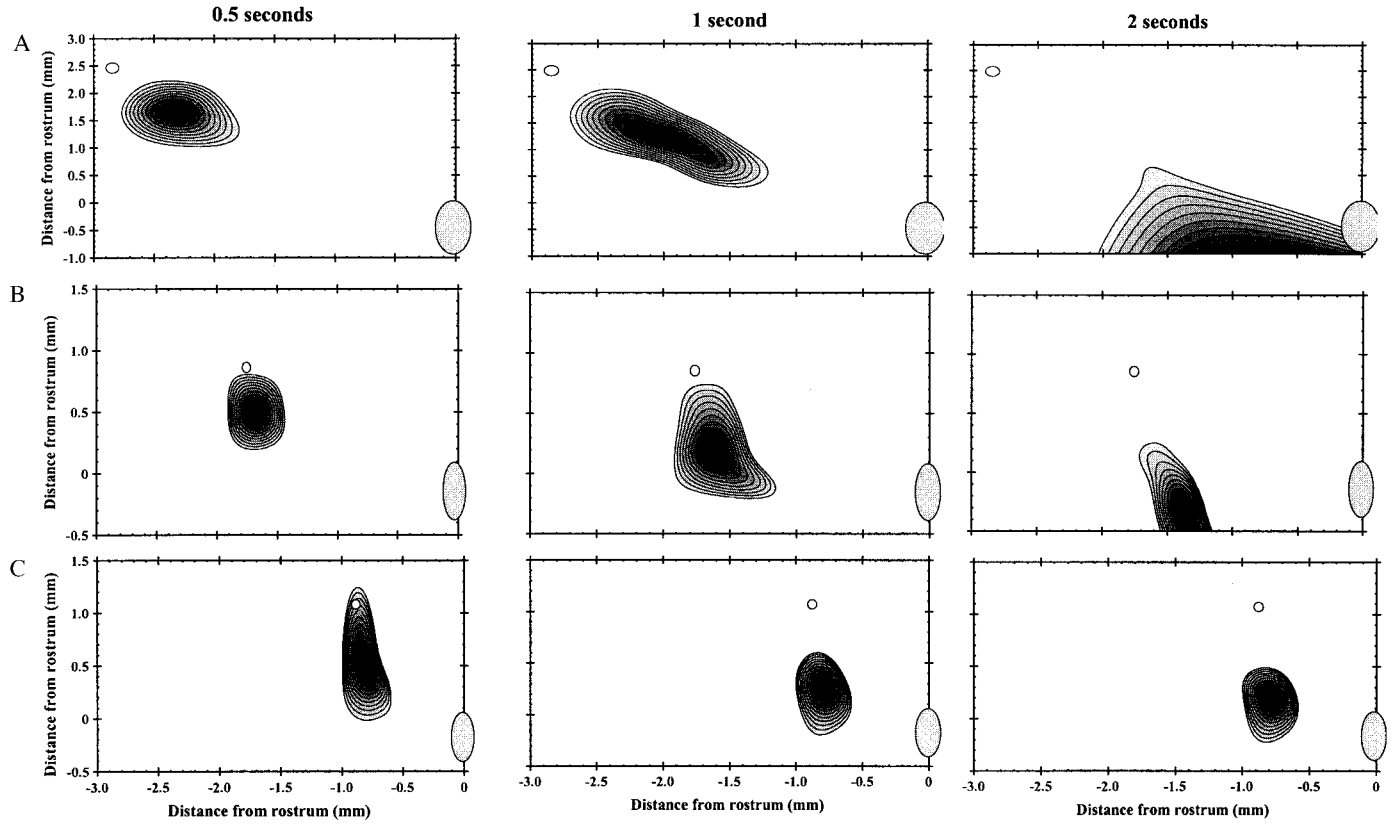

Fig. 7. Odor contours within the copepod feeding currents (copepod present with laminar advection, molecular diffusion, background convection, and pressure ejection acting). Top row (A) is for *P. xiphias* at 0.5, 1, and 2 s since time of ejection of odor bolus. Middle (B) and bottom (C) rows are *E. rimana* at the same time intervals. Contour lines are spaced at 10% intervals relative to the maximum concentration within each plot (the center). Open circle is location of the stimulus pipette. Note change in location between middle and bottom rows. The antennule of the copepod is located along the x-axis (at y = 0). All distances are shown as millimeters from the rostrum of the copepod. Note the change in the y-axis between the plots for *P. xiphias* and *E. rimana.* The gray oval represents of the body of the copepod.

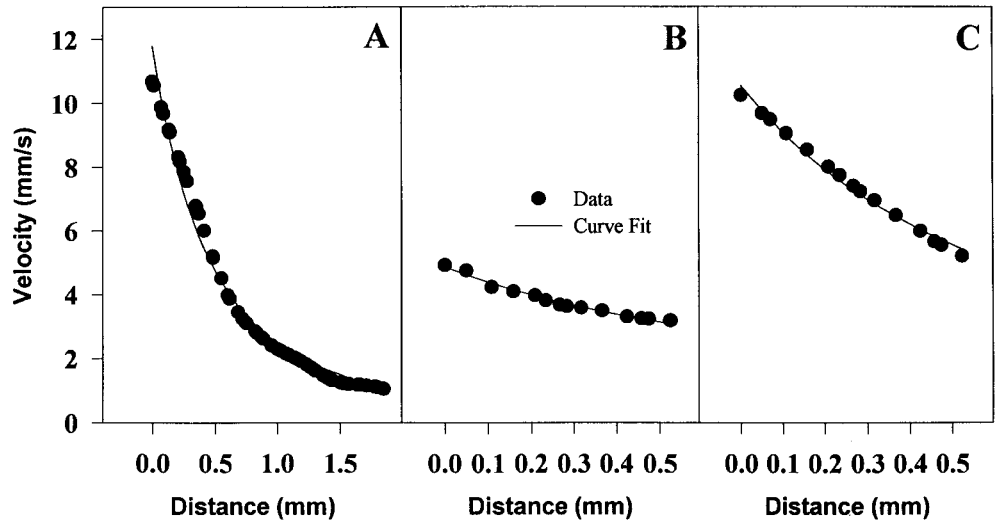

Fig. 8. Maximum fluid velocities along the plume path for (A) *P. xiphias,* and *E. rimana* (B, for distal pipette location and C, for proximal pipette location). Data points are derived from the flow field analysis, while solid line is derived from the statistical fit ($P > 0.98$ for all fits, chi-Squared analysis).

Table 2. Parameter estimates of forewarning values. Velocities within the feeding current, when fitted with Eq. 3, yield the following: the maximum velocity along the path (parameter *a*), the rate of decrease of that velocity (parameter *b*), the forewarning time (*c*), and the detection distance (*d*) for a copepod with a threshold sensitivity of 20% initial chemical concentration.

Animal	*a* (mm s^{-1})	*b*	*c* (ms)	*d* (mm)
Pleuromamma xiphias	11.8	−2.2	274	0.78
Euchaeta rimana (lateral)	4.9	−1.1	50	0.23
E. rimana (proximal)	10.5	−1.6	50	0.38

(*L*) of 750 μm for *P. xiphias* and 400 μm for *E. rimana.* This ratio indicates that the distribution of the chemical is strongly determined by advection, although solute transport by Fickian diffusion can not be ignored. In the absence of the pressure ejection of the chemical signal, we would expect the calculated diffusion coefficient to be up to one order of magnitude lower. This would result in a proportionally higher Peclet value.

Discussion

Foraging copepods can rely on chemoreception for the detection and location of potential prey items (Koehl and Strickler 1981; Poulet and Ouellet 1982). For example, *Eucalanus* sp. respond behaviorally to remotely detected chemical signals by diverting a streamline containing an algal cell when the cell was 1.25 mm distant (Koehl and Strickler 1981). Based on these observations, Andrews (1983) modeled a mechanism for the remote detection of particles. Andrews suggests that shear in a copepod's feeding current distorts the phycosphere surrounding an algal. If the copepod can sense the leading edge of the odor field, remote detection occurs. In general, our results support the model predictions of Andrew (1983). However, in the flow fields used in our study, we found a greater degree of longitudinal vs. transverse deformation of the sphere. Longitudinal stretching dominated odor distortion in Andrews' model, while we show, in all cases examined, that shear forces within the feeding current distort chemical signals both longitudinally and laterally along the copepod's antennules. As a result, the spatial and temporal distributions of the chemical signal are strongly influenced by the structure of the feeding current

Odor deformation in spatially variable velocity gradients—The structure of the chemical signal is highly dependent on the shear forces and velocity of the feeding current. Diffusion defines the initial gradient, while advection within the laminar feeding current distorts the shape of the odor field. Chemical signals located in high-shear feeding currents have spatial and temporal distributions different from signals located in lower shear flow fields. Chemical signals in high shear are more longitudinally stretched (Fig. 7), creating a longer distance from the leading edge of the chemical field to the center of the odor source. This longer distance provides the copepod with a greater lag time between detection and the time that the prey item enters its capture zone.

Using these feeding currents as models, a comparison of their structure suggests that a *P. xiphias*-type feeding current has greater potential for chemoreception based on estimates of early warning times. Our data (Figs. 4, 7) show that the phycosphere surrounding a food item will be more elongated when entrained by *P. xiphias* than by *E. rimana.* The 274-ms response time we found for *P. xiphias* was similar to the time found by Strickler (1982) of 430 ms for algal cell ingestion after detection 1.25 mm away. In contrast, assuming the same sensitivity, a copepod with the *E. rimana*-type feed-

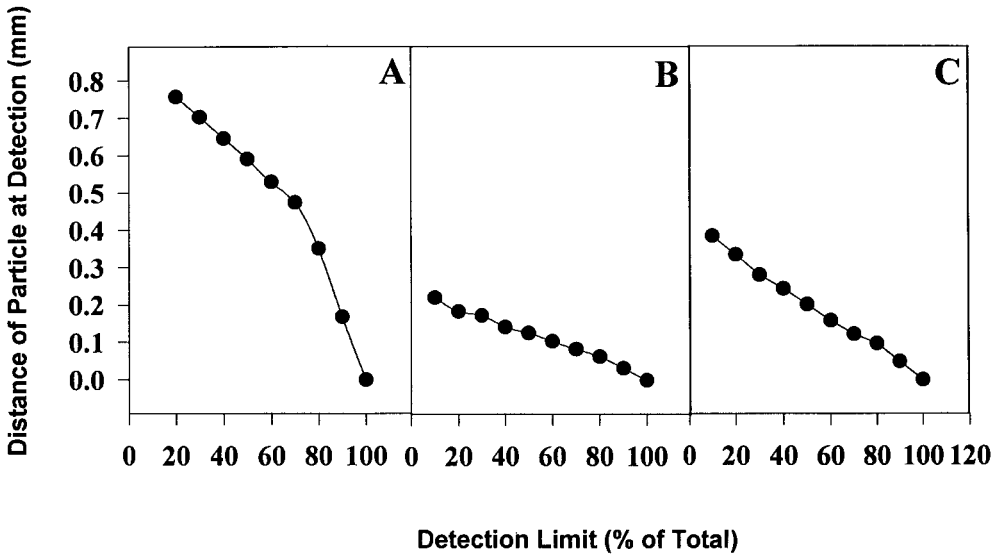

Fig. 9. Distance of the center of the chemical bolus from the copepod at time of detection as a function of detection ability. Detection ability plotted as percent of the maximum concentration of the chemical bolus. Detection distance for (A) *P. xiphias,* and *E. rimana* (B, for distal pipette location and C, for the proximal pipette location).

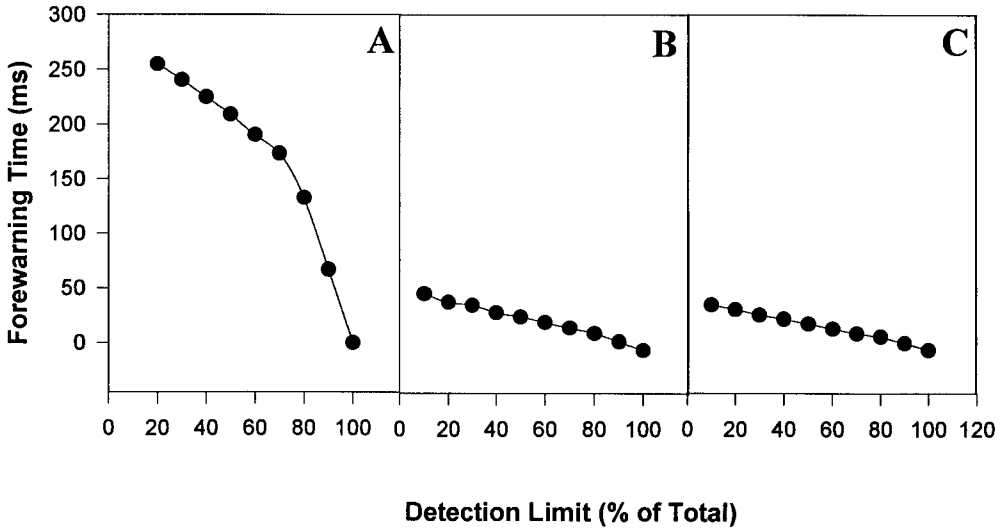

Fig. 10. Forewarning time as a function of detection ability of the copepod for (A) *P. xiphias,* and *E. rimana* (B, for distal pipette location and C, for proximal pipette location).

ing current has only 50 ms to respond to the presence of a chemical bolus. This difference is due to the distinctions between longitudinal and transverse shear in the feeding currents. Longitudinal shear increases the distance between the leading edge of the odor bolus and the center of the odor source, but since the whole odor field is experiencing acceleration, this increase in distance does not result in a concomitant increase in early warning time. With transverse shear, areas of the odor field are experiencing different velocities, such that increases in leading edge distances result in increases in early warning times. We recognize that flow velocities may be less and the maximal shear variations may be smoothed in the flow field of a free-swimming *P. xiphias* compared to that of a tethered copepod. However, our data show that feeding currents with high velocity and shear create the greatest separation of the leading edge of the odor field from the odor source and maximize the volume of water processed. Both are useful for copepods, such as *P. xiphias,* that often rely on detecting and gathering particulate algae for food.

Flows created by tethered *E. rimana* have low-shear values that were indistinguishable from those of free-swimming hovering copepods (Fields 1996). The low shear broadens the active space and has the potential of triggering numerous chemoreceptors on the antennules. However, this also reduces the capability to determine the exact location of the odor source. Such feeding currents, like *E. rimana's,* are more useful for copepods that forage upon mechanosensitive prey. Such carnivores appear to minimize their hydrodynamic disturbance so mechanosensitive prey do not perceive their feeding current. However, the trade-off for having such a feeding current structure may be a reduced ability for remote chemoreception.

Constraints for effective chemoreception—Our research has revealed the importance of small-scale structure in the velocity gradient of the copepod feeding current for the remote detection of odor sources. These sources could be prey, predators, or mates. Those organisms that maximize the time needed for decisions to feed, avoid predators, or reproduce are more likely to respond correctly to the signal, thus improving fitness. We can now define various constraints for using chemoreception by copepods.

We found that sheared flow maximizes the detection distance, the separation of the leading edge from its source, the algal cell. Accordingly, the most strategic location to place chemoreceptors along the antennules is where the sheared streamlines intersect the antennule. Assuming that the feeding current structures of a hovering and a tethered animal are similar (Fields 1996), then for *P. xiphias,* which hovers 60% of the time (Fields pers. obs.), the chemoreceptors should be located 0.25–0.75 mm distal of the cephalic insertion. Indeed, the antennules of *P. xiphias* have numerous chemoreceptors within that region. Hence, the sensory architecture confirms the hypothesis concerning the location of the receptors. A similar observation for mechanoreceptors supports the interplay of flow structure and sensor morphology. On the outer edge of the flow field, where minimal shear makes chemoreception less likely, the sensors are predominantly mechanoreceptors (Fields and Yen 1993; Lenz and Yen 1993). The species-specific flow field can define the best location for sensors of certain modalities.

In addition to highly sheared flow, low-flow speed maximizes forewarning time. However, for the signal to be useful, the reaction time must be less than the forewarning time. Yet to minimize the reaction time, flow must be fast. Fast flow acts to thin the boundary layer surrounding the chemosensory structures, which effectively shortens the diffusion time (Moore et al. 1991; Yen et al. 1998). Hence, the commonly found distribution of chemoreceptors in copepods is to have a maximum density in the proximal region of the antennule where the feeding current flow speed is the highest (Boxshall et al. 1998). This finding suggests that thinning the boundary layer is an important component for chemosensation to maximize the forewarning time.

Chemical signals in lower shear zones with greater lateral

distortion will pass over a larger section of the antennules in a much shorter time before the arrival of the potential prey item. If the copepod uses the leading edge of the chemical field for an estimate of arrival time of the prey item, these estimates will vary along the length of the antennules due to differences in the longitudinal deformation of the chemical field. In addition, if the copepod uses the concentration gradient across the chemical field (and antennules) as a source of information about the spatial location of the prey item, this estimate will also vary along the length of the antennules due to differences in shear rates.

Wehner (1987) proposed that sensory efficiency is improved when the biological filter matches the signal structure within the stimulus environment. By integrating the perception of signals of both modalities, the copepod may be able to filter out the differences in the spatial and temporal distribution of chemical and shear field information and accurately predict both the location and timing of prey items arriving in the capture zone. Defining the stimulus environment can lead to predictions on how copepods use signals to increase foraging efficiency and how well the sensory system of copepods has adapted to their stimulus environments. Studies to define the sensitivity of both chemoreceptors and mechanoreceptors and the strength of the signals would define perceptive volumes, an important parameter in our estimation of encounter rates and consequent feeding and population growth rates of plankton in the sea.

References

ADAMS, R. N. 1969. Electrochemistry at solid electrodes. Marcel Dekker.

ANDREWS, J. C. 1983. Deformation of the active space in the low Reynolds number feeding current of calanoid copepods. Can. J. Fish. Aquat. Sci. **40:** 1293–1302.

BOXSHALL, G. A., J. YEN, AND J. R. STRICKLER. 1998. Functional significance of the sexual dimorphism in the array of setation elements along the antennules of *Euchaeta rimana* Bradford. Bull. Mar. Sci. **61:** 387–398.

BUNDY, M. H., AND G. A. PAFFENHOFER. 1996. Analysis of flow fields associated with freely swimming calanoid copepods. Mar. Ecol. Prog. Ser. **133:** 99–113.

CANNON, H. G. 1928. On the feeding mechanisms of the copepods *Calanus finmarchicus* and Diaptomus gracilus. J. Exp. Biol. **6:** 131–144.

CARR, W. E. S. 1988. The molecular nature of chemical stimuli in the aquatic environment, p. 3–28. *In* J. Atema, A. N. Popper, R. R. Fay, and W. N. Travolga [eds.], Sensory biology of aquatic animals. Springer.

CSANADY, G. T. 1980. Turbulent diffusion in the environment. D. Reidel.

DOURDEVILLE, T. A. 1981. A physical and physiological analysis of near-field displacement reception by a calanoid copepod, *Centropages typicus* Kroyer. M.A. thesis, Boston Univ.

EMLET, R. B. 1990. Flow fields around ciliated larvae: Effects of natural and artificial tethers. Mar. Ecol. Prog. Ser. **63:** 221–225.

FIELDS, D. M. 1996. The interaction of calanoid copepods with a moving fluid environment: Implications for the role of feeding current morphology in predator–prey interactions. Ph.D. thesis, State Univ. of New York.

———, AND J. YEN. 1993. Outer limits and inner structure: The 3-dimensional flow field of *Pleuromamma xiphias* (Calanoida: Metridinidae). Bull. Mar. Sci. **53:** 84–95.

———, AND ———. 1997. The escape behavior of marine copepods in response to a quantifiable fluid mechanical disturbance. J. Plankton. Res. **19:** 1289–1304.

FRIEDMAN, M. M. 1980. Comparative morphology and functional significance of copepod receptors and oral structures, p. 185–197. *In* W. C. Kerfoot [ed.], Evolution and ecology of zooplankton communities. Univ. Press of New England.

GALLAGER, S. M. 1993. Hydrodynamic disturbances produced by small zooplankton: Case study for the veliger larva of a bivalve mollusc. J. Plankton Res. **15:** 1277–1296.

GERHARDT, G. A., G. M. ROSE, AND B. J. HOFFER. 1987. In vivo electrochemical demonstration of potassium-evoked monoamine release from rat cerebellum. J. Neurosci. Methods **22:** 147–159.

GILL, C. W., AND S. A. POULET. 1986. Utilization of a computerized micro-impedance system for study activity of copepod appendages. J. Exp. Mar. Biol. Ecol. **101:** 193–198.

———, AND ———. 1988. Response of copepods to dissolved free amino acids. Mar. Ecol. Prog. Ser. **43:** 269–276.

JACKSON, G. A. 1989. Simulation of bacterial attraction and adhesion to falling particles in an aquatic environment. Limnol. Oceanogr. **34:** 514–530.

KOEHL, M. A. R., AND J. R. STRICKLER. 1981. Copepod feeding currents: Food capture at low Reynolds number. Limnol. Oceanogr. **26:** 1062–1073.

LAZIER, J. R. N., AND K. H. MANN. 1989. Turbulence and the diffusive around small organisms. Deep-Sea Res. **36:** 1721–1733.

LENZ, P. H., AND J. YEN. 1993. Distal setal mechanoreceptors of the first antennae of marine copepods. Bull. Mar. Res. **53:** 170–179.

MOORE, P. A., J. ATEMA, AND G. A. GERHARDT. 1991. Fluid dynamics and microscale chemical movement in the chemosensory appendages of the lobster, *Homarus americanus*. Chem. Senses **16:** 663–674.

———, G. A. GERHARDT, AND J. ATEMA. 1989. High resolution spatio-temporal analysis of aquatic chemical signals using microelectrochemical electrodes. Chem. Senses **14:** 829–840.

OKUBO, A. 1980. Diffusion and ecological problems: Mathematical models. Springer.

POULET, S. A., AND P. MARSOT. 1978. Chemosensory grazing by marine calanoid copepods (Arthropoda: Crustacea). Science **200:** 1403–1405.

———, AND G. OUELLET. 1982. The role of amino acids in the chemosensory swarming and feeding of marine copepods. J. Plankton Res. **4:** 341–361.

ROTHSCHILD, B. S., AND T. R. OSBORN. 1988. Small-scale turbulence and plankton contact rates. J. Plankton Res. **10:** 465–474.

STRICKLER, J. R. 1982. Calanoid copepods, feeding currents, and the role of gravity. Science **218:** 158–160.

———. 1985. Feeding currents in calanoid copepods: Two new hypotheses. Soc. Exp. Biol. **1985:** 459–485.

———, AND A. K. BAL. 1973. Setae of the first antennae of the copepod *Cyclops scutifer* (Sars): Their structure and importance. Proc. Natl. Acad. Sci. USA **70:** 2656–2659.

———, AND J.-S. HWANG. 1997. Matched filters in long working distance microscopy of phase objects, p. 63–82. *In* J. L. Wu and P. C. Cheng [eds.], Focus on modern microscopy. World Publishing.

TISELIUS, P., AND P. R. JONSSON. 1990. Foraging behavior of six calanoid copepods: Observations and hydrodynamic analysis. Mar. Ecol. Prog. Ser. **66:** 23–33.

WEATHERBY, T. M., K. K. WONG, AND P. H. LENZ. 1994. Fine structure of the distal sensory setae on the first antennae of

Pleuromamma xiphias Giesbrecht (Copepoda). J. Crustac. Biol. **14:** 670–685.

WEHNER, R. 1987. ''Matched filters''—neural models of the external world. J. Comp. Physiol. **161:** 511–531.

WONG, C. K. 1996. Responses of copepods to hydromechanical stimuli. Crustaceana **69:** 853–859.

YEN, J., AND D. FIELDS. 1992. Escape responses of *Acartia hudsonica* nauplii from the flow field of *Temora longicornis*. Arch. Hydrobiol. Beih. **36:** 123–134.

———, P. H. LENZ, D. V. GASSIE, AND D. K. HARTLINE. 1992. Mechanoreception in marine copepods: Electrophysiological studies on the first antennae. J. Plankton Res. **14:** 495–512.

———, AND N. T. NICOLL. 1990. Setal array on the first antennae of a carnivorous marine copepod, *Euchaeta norvegica*. J. Crustac. Biol. **10:** 218–224.

———, B. SANDERSON, J. R. STRICKLER, AND A. OKUBO. 1991. Feeding currents and energy dissipation by *Euchaeta rimana*, a subtropical pelagic copepod. Limnol. Oceanogr. **36:** 362–369.

———, AND J. R. STRICKLER. 1996. Advertisement and concealment in the plankton: What makes a copepod hydrodynamically conspicuous. Invertebr. Biol. **115:** 191–205.

———, M. J. WEISSBURG, AND M. H. DOALL. 1998. The fluid physics of signal perception by mate-tracking copepods. Philos. Trans. R. Soc. Lond. B **353:** 787–804.

ZARET, R. E. 1980. Zooplankters and their interactions with water, with each other, and their predators. Ph.D. dissertation, The John Hopkins Univ.

Received: 23 October 1997
Accepted: 12 August 1998
Amended: 22 September 1998